Fine and ultrafine particles at a near–free tropospheric environment over the high-altitude station Hanle in the Trans-Himalaya: New particle formation and size distribution

K. Krishna Moorthy,[1] V. Sreekanth,[1] Jai Prakash Chaubey,[1] Mukunda M. Gogoi,[1] S. Suresh Babu,[1] Sobhan Kumar Kompalli,[1] S. P. Bagare,[2] Bhuvan C. Bhatt,[2] Vinod K. Gaur,[2] T. P. Prabhu,[2] and N. S. Singh[2]

Received 6 June 2011; revised 9 August 2011; accepted 9 August 2011; published 27 October 2011.

[1] Number-size distributions of ultrafine, fine, and accumulation mode aerosols in the size range 5–1300 nm have been measured regularly from the pristine, high-altitude (for 4520 m above mean sea level) station Hanle in the Trans-Himalaya during the summer and autumn (August–November) 2009. The total number concentration ranged from 80 to 8000 cm^{-3} with a mean value of 1150 cm^{-3}. Examination of the temporal variations of the size distributions indicated that formation of new ultrafine particles from the precursor gases (probably transported from the valley regions) was highly probable during the forenoon hours of the day, especially during the summer when the insolation was abundant, the process becoming increasingly less efficient as the season progressed toward winter. The time of occurrence of maximum concentration was generally during the forenoon, a few hours after sunrise, and this time shifted to later parts of the day as the season progressed toward winter, probably associated with later sunrise and low solar elevations. The number-size distributions revealed two prominent modes: a nucleation mode with mode diameter at ~16 nm and a consistent accumulation mode with the mode diameter ranging between 115 and 150 nm. Examining the temporal features with the air mass types, it was noticed that the number concentration increased, and the accumulation mode broadened when west Asian air mass prevailed. In summer (during August) the number concentrations tended to higher values associated with air mass from the Indian origin. The ratio of the Aitken to accumulation mode concentration indicated that the aerosol particles existing over the site are aged.

Citation: Moorthy, K. K., et al. (2011), Fine and ultrafine particles at a near–free tropospheric environment over the high-altitude station Hanle in the Trans-Himalaya: New particle formation and size distribution, *J. Geophys. Res.*, *116*, D20212, doi:10.1029/2011JD016343.

1. Introduction

[2] The spatiotemporal heterogeneity in aerosol characteristics and radiative forcing even at regional scales, the inadequate regional representation of aerosol characteristics in models and the limitations of the models to incorporate the aerosol-climate feedbacks with sufficient accuracy remain the major challenges in accurate assessment of the climate impact of aerosols [*Remer et al.*, 2009]. In this context, improved knowledge of aerosol abundance (number concentration) and size distribution and their variabilities remain one of the important information well sought after, for estimating either the direct radiative forcing or in understanding aerosol-cloud interactions and resulting indirect climatic effects [*Jiang and Feingold*, 2006; *Fan et al.*, 2007]. Viewed in the above perspective, information from high-altitude and pristine locations assumes great importance as it provides a sort of background, against which the human impacts could be compared. Besides, long-term changes in aerosol characteristics in these regions would be indicative of probable global trends and impacts at much larger scales. *Weingartner et al.* [1999] and *Shaw* [2007] have hypothesized that the free troposphere would act as a reservoir for several gaseous species, which form new particles through gas-to-particle conversion mechanisms under favorable conditions such as availability of moisture and UV radiation), thereby making this region conducive for examining aged as well as new particles coexisting. High-altitude observatories come handy in this context, with the availability of abundant UV radiation (since nearly half the atmosphere is below the measurement

[1]Space Physics Laboratory, Vikram Sarabhai Space Centre, Trivandrum, India.
[2]Indian Institute of Astrophysics, Bangalore, India.

0148-0227/11/2011JD016343

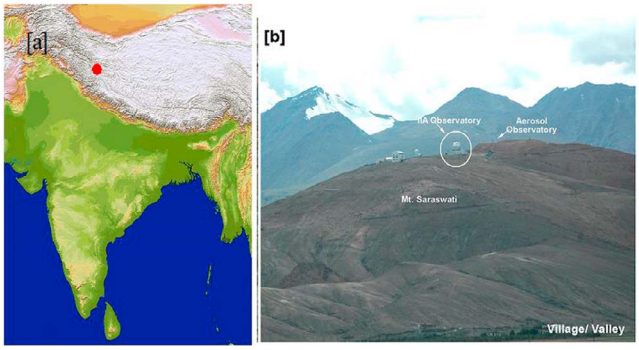

Figure 1. (a) Geographical location of Hanle (marked by the red circle) superimposed on the digital elevation map of the Indian subcontinent. (b) Long-shot picture showing the aerosol observatory on Mt. Saraswati along with the Indian Institute of Astrophysics (IIA) observatory. The relative location of the village in the valley region can also be seen.

level) to initiate photolysis reactions when enough water vapor/OH and precursors are also available.

[3] Recent airborne measurements during the Integrated Campaign for Aerosols, Gases and Radiation Budget (ICARB) [*Moorthy et al.*, 2008] field campaign over Indian subcontinent and surrounding oceanic regions have revealed that during premonsoon season, most of Indian region is characterized by elevated aerosol layers, occurring in the altitude range of 2 to 5 km, within which the aerosol loading and extinction were larger than those observed close to the surface and within the atmospheric boundary layer [*Babu et al.*, 2008, 2010; *Satheesh et al.*, 2008, 2009a, 2009b]. From the airborne measurements of number-size distribution off Bhubaneswar (20.23°N, 85.82°E) over the northern Bay of Bengal using scanning mobility particle sizer (SMPS), *Murugavel et al.* [2008] reported a peak in the number concentration of aerosols above the atmospheric boundary layer and attributed this to the combined effect of advection and new particle formation in this moderately humid region. On the basis of measurements and modeling, *Satheesh et al.* [2008] have reported a meridional gradient in the lower atmospheric warming by aerosol absorption over the Indian landmass. From numerical simulations, *Lau et al.* [2006] and *Lau and Kim* [2006] have shown that absorption of solar radiation by aerosols (dust and black carbon) and the consequent warming over Tibetan Plateau would act like an "elevated heat pump (EHP)," which would draw in warm and moist air over the Indian sub continent leading to modifications of the Indian summer monsoon. In the backdrop of all the above, with a view to examining and quantifying the meridional gradient in the elevated warming up to the Himalayan regions, a field experiment RAWEX (Regional Aerosol Warming Experiment) has been formulated under ISRO-GBP (Indian Space Research Organization–Geosphere Biosphere Programme) focusing on observations from the locations situated in and around the Himalayas in conjunction with the measurements from the network of ground stations in the plains. During the first phase of RAWEX, an aerosol observatory was setup in August 2009, at Hanle, a high-altitude remote location in the Trans-Himalayan region at an altitude of ~4520 m above mean sea level where several parameters of aerosols are being monitored regularly. In this paper we present the results of the number-size distribution measurements carried out from Hanle during the period from August to November 2009.

2. Site Description and Meteorological Conditions

[4] The measurements were carried out from the premises of the Himalayan Chandra Telescope site (see http://www.iiap.res.in/iao/iao.html) of the Indian Institute of Astrophysics, atop Mt. Saraswati (32.78°N, 78.96°E), at an altitude of ~4520 m amsl (above mean sea level), located in the Hanle valley (~4250 m amsl) in the Trans-Himalayan region, to the west of the Tibetan plateau (Figure 1). The peak is surrounded by several similar or taller peaks, all maintaining a natural environment of sparse vegetation and arid regions akin to a tall mountain desert. The taller peaks around Mt. Saraswati remain snow-capped even during peak summer and snow covered in winter. The population density within the valley and surrounding areas is around ~10 km^{-2}, except for some pockets of military campsites the nearest by ~20 km northwest of the Hanle valley. Even the lightly inhabited areas lay downwind of the measurement site for most of the year. Yak and sheep grazing is the main activity during summer and autumn, with a little small agricultural activity in the valley area by the few local population. With these features, and being located far remote from any major anthropogenic sources of pollution and at an altitude >4.5 km, the site could be considered as a virtual free-tropospheric site with highly subdued local interference.

[5] In general, the site is significantly dry throughout the year with very low precipitation of <10 cm annually [*Verma et al.*, 2009]. The daily mean values of the temperature, relative humidity (RH), wind speed and pressure for the study period are shown in Figures 2a–2d. These parameters are obtained from the high-resolution (one second) automatic weather station (AWS) measurements, which was under continuous operation during the study period. The vertical bars in Figure 2 indicate the variability (standard deviation) of the particular parameter within a day. During the study period, temperature decreased monotonically from August to November with a maximum value of ~16°C (occurring in August) and a minimum value of −12°C (in November). RH did not show any trend; rather fluctuated about a mean value of 30%, which is in line with that reported by *Verma et al.* [2009] for yearly mean. Daily mean winds were high over the region, ranging from 1 to 15 m s^{-1} with a long-term mean value of ~5 m s^{-1}. The atmospheric (surface) pressure values lay between 585 and 595 mb throughout the study period. During the first half of September, the station experienced an intense snowfall episode with continuous snowing for about 4 to 5 days. During this episode, the temperatures dropped (as shown by downward arrows in Figure 2, between Julian days 250 and 258), almost reaching to 0°C, associated with abrupt peaking in the RH values (~90%). Also, very calm wind conditions prevailed all through the snow episode with the daily mean winds speeds coming down to as low as ~1 m s^{-1}. Other than this, there was no precipitation recorded during the mea-

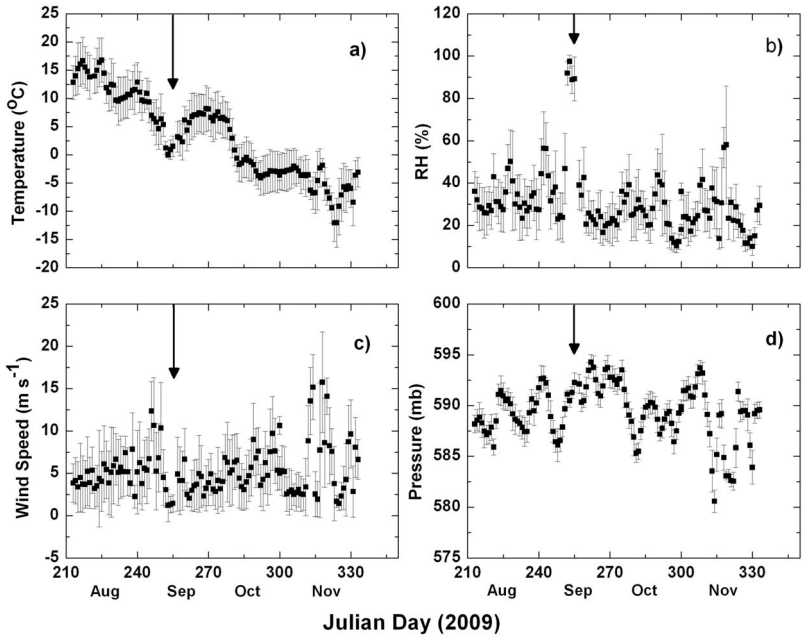

Figure 2. Daily mean values of the surface meteorological parameters: (a) air temperature, (b) relative humidity (RH), (c) wind speed, and (d) pressure. Error bars indicate the standard deviations. Downward arrows indicate a snowfall event (rare occurrence) during September 2009 which persisted for a few days. An abrupt increase in RH values and a decrease in temperature and wind speed can be observed and associated with these events.

surement period. The wind direction has been predominantly southwesterly (Figure 3) during the study period. Owing to the prevailing dry and cold meteorological conditions, Hanle and its surrounding valley areas are often termed as "cold desert."

[6] Diurnally, the ambient temperature maximized at ~15:00 local time (LT), while the lowest value occurred at ~06:30 LT. Lowest RH values occurred during the noontime and highest in the morning hours. The winds follow general pattern, starting with a mild wind at the early hours of the day, picking up gradually and reaching the peak values of up to 15–20 m s^{-1} in the afternoon, so that the afternoons and evenings are in general more windy than the forenoons.

3. Instrument and Data

[7] Number-size distribution measurements of ambient aerosols were carried out using a Sequential Mobility Particle Sizer + Counter (SMPS+C) of GRIMM Aerosol tek GmbH, Germany that was installed at the mountaintop. The instrument segregates particles from the air stream in terms of their differences in electrical mobility at small increments using a Differential Mobility Analyzer (DMA) classifier [*Collins et al.*, 2004] and references therein) and transfers them to a Condensation Particle Counter (GRIMM 5.400) for counting. The DMA was operated at sheath and sample airflow rates at 2 and 0.2 L per minute (LPM), respectively, and used an Americium (AM 241) alpha source to bring the particles to equilibrium charge distribution. Depending on the type of DMA used, the instrument classifies particles in the size range from 15.9 to 1363.6 nm (LDMA), or from 8.9 to 552 nm (UDMA); in both the cases into 44 size classes, the geometric mean diameters of these classes being distributed evenly in a logarithmic scale. More details are available in the work of *Reischl* [1991].

[8] The CPC basically works on the principle that the monodisperse aerosol flow from the DMA classifier passes over a warm reservoir of N-Butanol (Butyl alcohol C_4H_9OH) where it becomes saturated with a condensable vapor. During subsequent cooling in the condenser chamber,

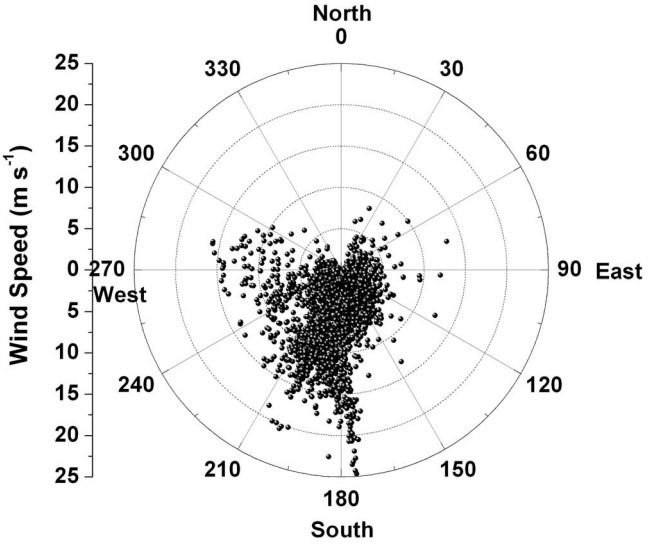

Figure 3. Mass plot of the instantaneous surface wind speed and direction during the study period.

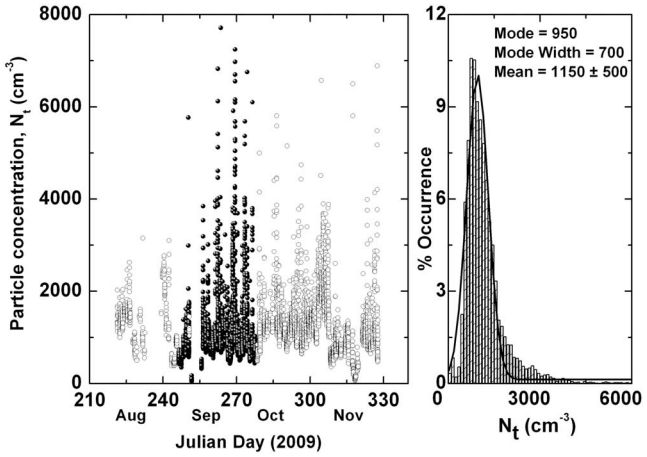

Figure 4. (left) Time series of the particle number concentrations (N_t). Open and solid circles indicate data collected using the LDMA and UDMA, respectively. (right) Frequency distribution of the number concentration is shown as bars, and the solid line represents the best fit Gaussian distribution.

the vapor becomes supersaturated, causing particles to grow into large droplets, which are individually counted using light scattering. The analysis of the raw data thus obtained was carried out using the software supplied by the manufacturer. During the study period, we have used both the DMAs to examine the size distributions (the rationale for which are discussed in section 5); however only one at a time as we had only a single CPC. The instrument has been operated daily (except on days of snowfall or on days when there were local activities in and around the station) from ~08:00 LT to 18:00 LT during August to November 2009. Beyond 18:00 LT, the ambient temperature dropped too low to operate the instrument. The sample air was drawn into the instrument from an inlet at 2 m above the ground through a 1 m electrically conductive resinous tube.

4. Analysis of the Data and Deduction of Aerosol Parameters

[9] While the instrument provided one size spectrum roughly every 6 min, which also included the total count and the geometrical mean radius (GMR) of the size spectrum (GMR = $\sqrt{r_a r_b}$, where r_a and r_b are respective radii limits of the classifier bins. Other physically meaningful parameters of aerosols, such as the number of modes, mode radii have been determined for the individual spectra, separately during offline analysis. For this, each of the number-size distribution was analytically described as a sum of two or three lognormal functions distributions, using the expression

$$\frac{dN}{d\ln D_p} = \sum_{i=1}^{n} \frac{N_i}{\sqrt{2\pi}\ln\sigma_{g,i}} \exp\left[-\frac{\left(\ln D_p - \ln D_{g,p,i}\right)^2}{2\ln\sigma_{g,i}}\right] \quad (1)$$

so as to get minimum root-mean-square (RMS) deviations between the measured and analytically fitted spectra. In equation (1), D_p is the particle diameter, n is the total number of modes considered, $D_{g,p,i}$ is the geometric mean diameter of the ith mode (i varying from 2 to 3 as mentioned above), $\sigma_{g,i}$ the corresponding geometric standard deviation of the mode, and N_i is the particle number concentration of the ith mode. Following the convention of *Raes et al.* [2000], we considered the following three modes: nucleation mode (particle diameter <50 nm) Aitken mode diameter both 50 and 100 nm and accumulation mode $D_{p,g}$ > 100 nm. Accordingly, we also estimated the number concentration of particles N_i for each mode regime. In all we had ~8000 spectra during the measurement period, which were analyzed as detailed above.

5. Results

5.1. Total Number Concentrations (N_t) and Geometric Mean Diameter (G_d)

[10] The time series of the total number concentrations (N_t), derived from each scan of the SMPS, is shown in Figure 4 (left), for the period from August to November 2009, in which each point corresponds to one spectrum and the time is converted to fraction of the Julian day. Figure 4 (right) shows the frequency distribution of N_t with the solid line indicating the best fit, with a squared correlation coefficient of 0.95 and RMS error of 41.9. The mean and median (mode) values are also written in Figure 4. Even though N_t varied over a wide range (from as low as 80 cm^{-3} to as high as 8000 cm^{-3}), the frequency distribution was unimodal with a median value (mode) at ~950 cm^{-3}, while the mean concentration was higher (~1150 cm^{-3}) indicating a skewed distribution; with the few very high concentrations (occurring occasionally) contributing to the mean. Examining the monthly pattern, it was noticed that highest mean N_t values occurred in August (~1400 cm^{-3}) and the least value occurred in September (~900 cm^{-3}) during the first half of which the station experienced an episode of strong snowfall. During October and November, the means remained around the entire data average of 1150 cm^{-3}. Examining our values against those reported from similar altitudes, it is noted that *Sellegri et al.* [2010], on the basis of long-term measurements at the high-altitude Himalayan site of Nepal Climate Observatory-Pyramid (NCO-P, 27.95°N, 86.82°E, 5079 m asl), have reported an annual mean concentration of ~850 cm^{-3} having a strong seasonality (with a premonsoon (spring) high value of ~1500 cm^{-3} and postmonsoon (Autumn) value of ~1300 cm^{-3} with the monsoon minimum), which are generally comparable to our values for the similar seasons. However, higher concentrations have been reported from lower-altitude Himalayan stations. For example, *Komppula et al.* [2009], on the basis of 3 years of observations from Mukteshwar (2180 m amsl), a location toward southeast of Hanle reported that the monthly averages of N_t varied from 5700 cm^{-3} in spring to about 1200 cm^{-3} during the rainy (summer) season. *Gajananda et al.* [2005] have reported concentrations at three altitude levels ranging from 1150 to 2530 m amsl in the northwestern part of Himalayas with mean concentrations of 4350 and 1390 cm^{-3} at the lowest- and highest-altitude levels. It may be kept in mind that in addition to being from lower-altitude regions (compared to Hanle), the values of *Gajananda et al.* [2005] corresponded only to particle sizes >100 nm which excluded numerous particles occurring below 100 nm.

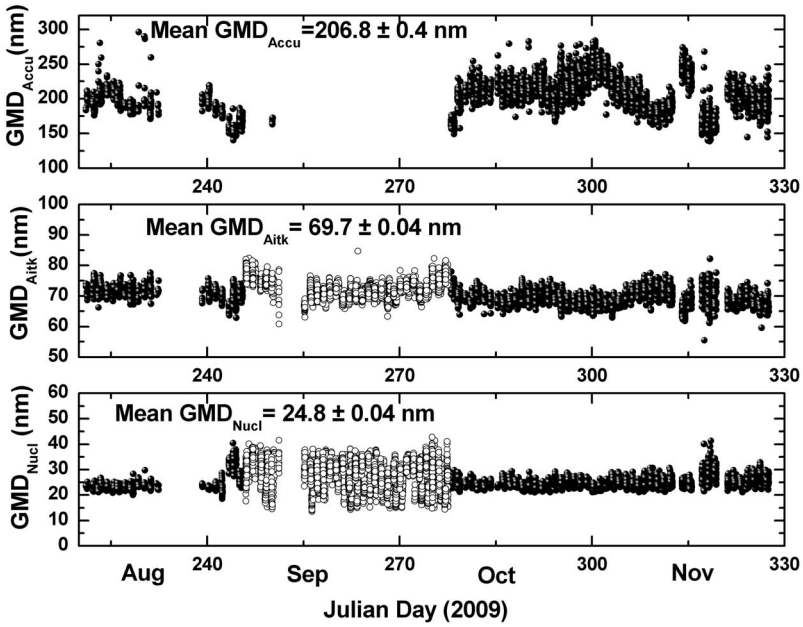

Figure 5. Temporal variation of the geometric mean diameter (GMD) for (top) accumulation, (middle) Aitken, and (bottom) nucleation regimes. Solid and open circles indicate data collected using the LDMA and UDMA, respectively.

[11] Geometric mean diameter (GMD, G_d) has been estimated as the exponential of the weighted mean of the aerosol size distribution against the variable ln (D_{pi})

$$G_d = \exp\left[\frac{\sum_i n_i * \ln D_{pi}}{N}\right] \quad (2)$$

where n_i is the number of particles in the ith size interval, D_{pi} is the midpoint of the size diameter and N is the total number concentration. The temporal variation of the mode diameters of the regimes considered in this study, for the data period, is shown in Figure 5, which shows that rather stable nature of the modes over the period of study with mean values of 24.8 ± 0.04, 69.7 ± 0.04, and 206.8 ± 0.4 nm for nucleation, Aitken, and accumulation modes, respectively. Extending the analysis to the entire size distribution, the temporal variation of the mode diameter of the size distribution and the frequency distribution are shown in Figure 6, following the same conventions as in Figure 4. In general, G_d ranged from 20 nm (when the size distributions exhibited high nucleation events) to 125 nm with an average value of 61 ± 13 nm, while the frequency distribution of the mode is sharply peaked with a median value of 60 nm. Examining the monthly means, the month of August showed slightly higher values of G_d (~70 ± 10 nm) than the other three months (~60 ± 15 nm). Notwithstanding that both G_d and N_t were high in August, a scatterplot between N_t and G_d (Figure 7) revealed a general decrease in G_d with increase in N_t, suggesting that large contribution to N_t comes from nucleation and Aitken mode particles. This in turn, suggests new particle formation, which generally fall in very low size range of 1 to 3 nm, over the site. *Komppula et al.* [2009] have found good association between a decrease in G_d and new particle formation from gaseous precursors, while *Kulmala et al.* [2004] have reported that the new particle formation from gas phase reactions occurs generally in the 1 to 3 nm size range. As the minimum detectable size range of our instrument is >8 nm, such processes would be captured by our measurements only after a certain amount of growth.

[12] It is generally accepted that the new particle formation in the atmosphere occurs via homogeneous heteromolecular nucleation process, in which two or more vapor species react to form new products, which nucleate in to stable particles [*Kulmala et al.*, 2004]. The main species responsible for atmospheric nucleation and early particle growth is believed to be sulphuric acid (H_2SO_4), which is

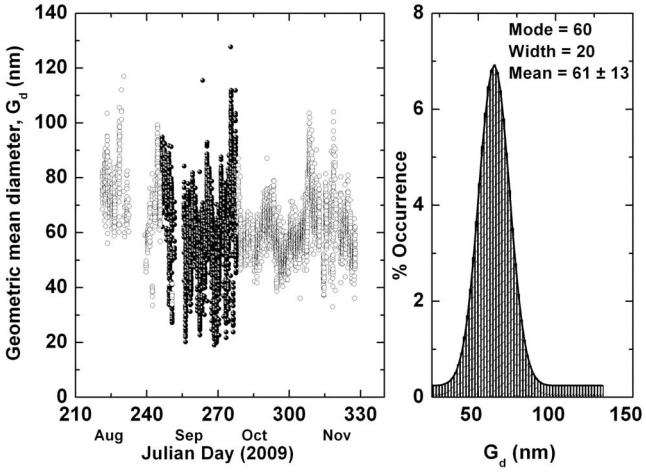

Figure 6. Same as Figure 4 but for geometric mean diameter (G_d).

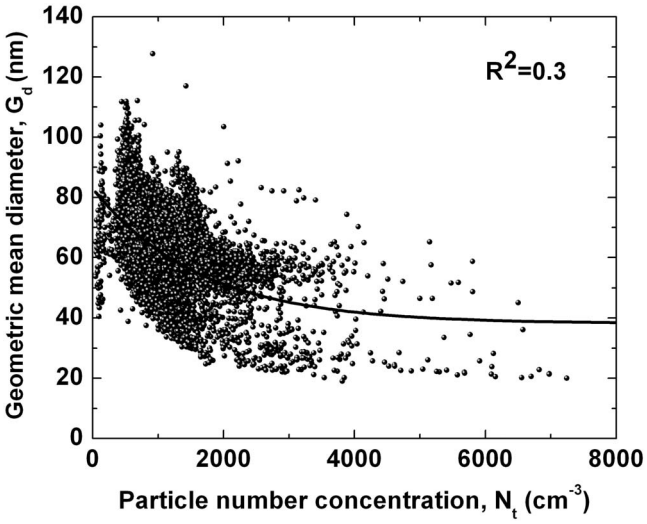

Figure 7. Relation between particle number concentration (N_t) and geometric mean diameter (G_d). Solid line indicates the best fit trend.

known to conucleate very efficiently with water vapor through binary nucleation processes [*Hamed et al.*, 2011]. Bursts of new particle formation have been observed in the free troposphere [*Raes et al.*, 1997; *Weber et al.*, 1995], and under very low RH conditions over continental locations [e.g., *Vaattovaara et al.*, 2009]. In a recent study, on the basis of observations, theoretical calculations and model simulations, *Hamed et al.* [2011] have demonstrated an anticorrelation between RH and new particle formation over several continental locations. Some of the reasons put forth include: (1) enhanced coagulation scavenging of the freshly nucleated particles at high RH, (2) diminished solar radiation at high RH (increased haze and cloud cover) leading to weaker gas-phase reactions, (3) increased condensation sink of condensable gases due to hygroscopic growth of the preexisting particles. In the context of Hanle, a dry location at free tropospheric heights (with almost half the atmosphere below) the ambient relative humidity is generally very low (~30%) throughout the year and solar radiation (including UV) is abundant especially in late spring and summer. This creates conditions quite conducive for new particle formation from gaseous precursors, through photochemistry, being supported by the thermal wind circulation bringing in the precursor gases from the valleys (near and far). Increased thermal convection in these seasons are capable of bringing in higher concentration of precursor gases and insoluble organic compounds from the lower altitudes, which further the photochemistry as has been suggested by *Lee et al.* [2008]. *Brown et al.* [2006] have suggested that oxidation of SO_2 to H_2SO_4 by species such as NO_3 could occur in polluted continental plumes, where these species are abundant.

[13] With a view to investigating it further, we examined the diurnal variation of N_t and G_d and its day-to-day changes in Figure 8. Figure 8a clearly shows that during August, despite N_t remaining fairly high, there were no preferred times for its maximum or minimum. However, from the second half of September (Julian day 260) onward, occurrences of several "hot spots" are noticed during forenoon periods, when the N_t values go very high, shooting up to ~5000 cm^{-3}, compared to the more benign afternoon values. It is interesting to note that, the temporal variations of G_d, shown in Figure 8b, exhibit conspicuous minima, almost corresponding to these hot spots, indicating that the large increase in the number concentration is almost associated with a large increase in the abundance of nucleation and Aitken mode particles, thereby resulting in the large decrease in G_d. This is confirmed in Figure 8c, which shows the temporal variations of the combined number concentration of particles in the nucleation and Aitken modes (diameter less than 100 nm). These temporal variations are very similar to those seen in N_t, with sharp enhancements (up to ~2000 cm^{-3}) in conjunction with the hot spots in Figure 8a. Both these features occurred invariably during the forenoon period; between 08:00 and 12:00 LT; being earlier in September, and shifting gradually to later parts of the forenoon as the days advanced. For example, while in September, the diurnal peak occurred at ~09:00 LT, by November the time of occurrence of the peak was as late as

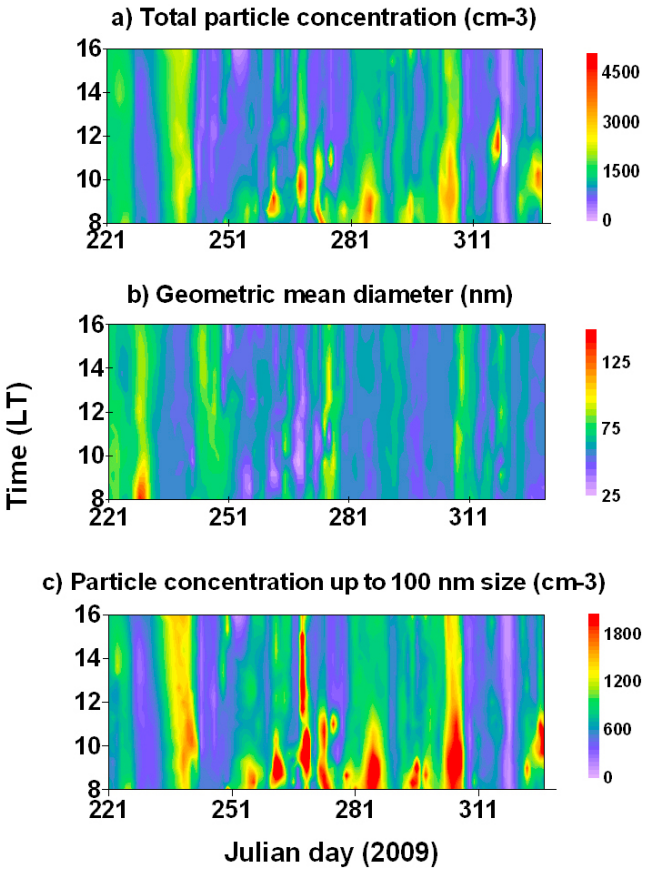

Figure 8. Temporal variations (diurnal and day to day) of (a) total number concentration, (b) geometric mean diameter, and (c) particle concentrations below 100 nm diameter. Note the strong peaks in N_t during the forenoon hours from Julian day 260 onward, suggesting large abundance of particles. During the same periods, Figure 8b shows a large reduction in G_d, suggesting that the increase in N_t is mainly due to a large increase in the nucleation and Aitken mode particles, possibly associated with new particle formation from precursors.

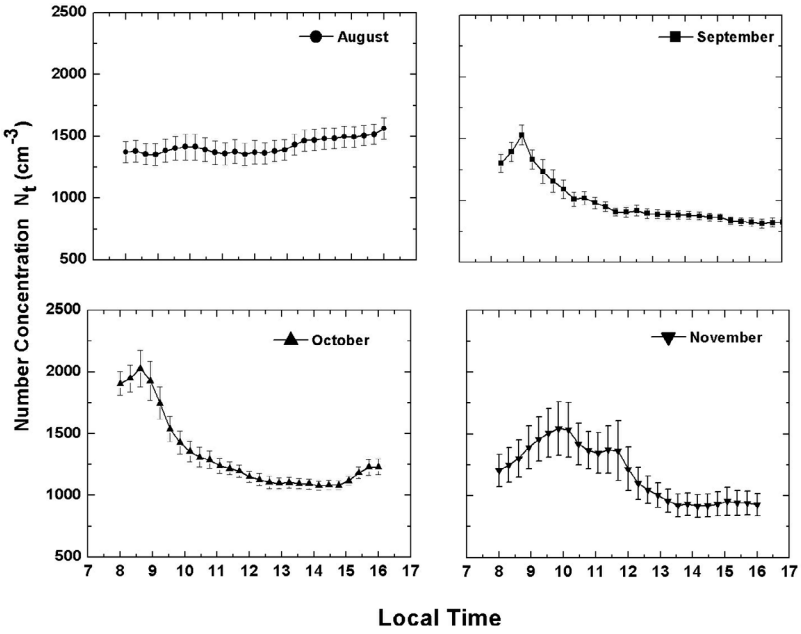

Figure 9. Monthly mean diurnal variation of the particle number concentration. Error bars indicate the standard error in the mean values. A gradual shift to the later hours is seen in the occurrence time of the peak.

~11:30 LT. Nevertheless, the peaks occurred always in the forenoon period. As the local sunrise shifts toward later hours as the days progressed, being at 05:37 in August, 05:57 in September, 06:17 in October and 06:43 in November (where the times represent the sunrise time for the 15th of each month) and the solar radiation reached at increasingly low elevation angles. The above observations are strong indicators of photochemical production of new particles leading to the hot spots. A similar observation has been made by *Shaw* [2007] on the basis of a 4 month long database (February to May 2002) over Mt. Lemmon (2790 m asl) in Arizona, with a systematic shift in the time of the maximum aerosol concentration in the diameter range 20 to 40 nm (nucleation mode) with advance of the season; occurring earlier in the day during later parts of the spring, as the solar radiation intensity increases. Here it is to be noted that the measurement at Mt. Lemmon (almost at the same latitude as Hanle) were made during the winter and spring seasons (when the solar elevations in the mornings would be much lower to start with and gradually increasing as the season progresses) where as the measurement over Hanle were made during the period Summer (when the solar elevations are higher) to Autumn (decreasing gradually). As such, the evidence of nucleation events at Hanle that shows up in the morning hours during August–September, shifts gradually to the later hours (closer to noon) toward November, in line with the gradual decrease in the solar elevation and more similar to those seen at Mt. Lemmon. Thus there is a seasonality in the diurnal evolution of the nucleation event and it appears to be associated with the solar elevation, which eventually influences the amount of UV radiation. It thus appears that photochemical reactions involving gaseous precursors, in presence of the moderate relative humidity of the morning hours and the availability of abundant solar (UV) radiation at the high-altitude location (of 4.5 km above mean seal level (msl)) of Hanle are conducive for generation of new particles in the nm size regime. (However, we did not have the measurements of UV radiation to confirm this.) The subsequent growth by coagulation and condensation (of vapors) make these particles detectable by the SMPS. The availability of the precursor gases is probably ensured by the strong westerlies/southwesterlies that prevail during this period, which favor advection from the inhabited region of west Asia, Europe, besides from the southwestern parts of India. This aspect is examined later.

[14] The monthly mean diurnal variation of N_t for the months of September to November, shown in Figure 9, is consistent with the above; with a gradual increase from the morning hours to reach the peak, the time of occurrence of which shifts to later hours with months, and then starts decreasing to reach a minimum value at ~16:00 LT. The large variation in N_t around the peak (as shown by the standard deviations) indicates the transient nature of these newborn particles. The role of valley and mountain breeze activity in bringing up particles and precursor gases from the valley (inhabited, though sparsely), respectively, to the measurement sites on hilltops in the morning, and taking down the particles from the top to the valley in the evening would also be contributing significantly to the observed diurnal variations, as has also been discussed by *Sellegri et al.* [2010]. This also makes the high-altitude peaks more pristine during nights [*Shaw*, 2007]. Shaw has also proposed the idea of a virtual layer, above the temperature inversion, which "pollutes" the upper regions during daytime, by convective mixing. Examining Hanle results in this light, it is noted that Hanle is at 4520 m msl (as against Mt. Lemmon ~2790 msl). Moreover Hanle is not a tall peak in an other-

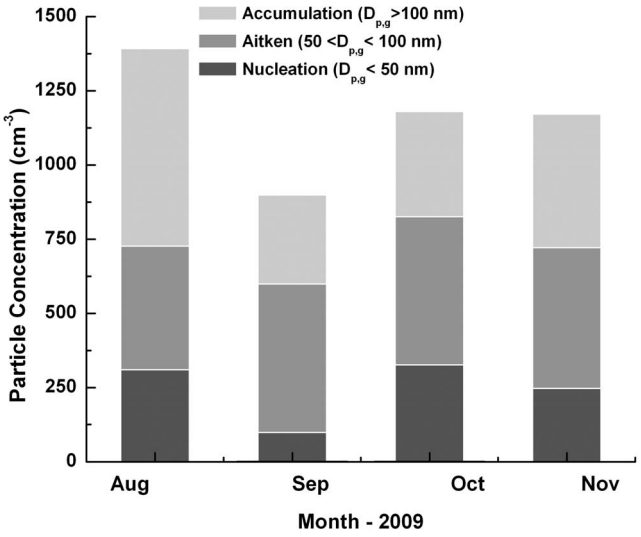

Figure 10. Stacked histogram of monthly mean particle concentrations in the accumulation, Aitken, and nucleation regimes. Total height of the histogram represents the monthly mean total particle number concentration.

wise plain region, but a small peak in an elevated mountain region of the Trans-Himalaya, with several similar peaks around on the valleys that are poorly inhabited. These peaks, spread over several hundred kilometers north-south provide an orographic barrier for the transport of pollutants lifted by convection from the southern plains. This is also borne out by the cluster analysis (later). However, locally over the Trans-Himalaya, convection could reach the peak during summer pushing up the small amounts of pollutants from the sparsely inhabited valleys, creating some sort of a virtual layer, where the precursor gases would reside.

[15] To examine this aspect further, we considered three particles regimes within the size range of measurements; the nucleation mode (particle diameter <50 nm); the Aitken mode (50 nm < diameter < 100 nm); and accumulation mode (diameter >100 nm) as defined in section 4 and estimated the concentration in each of these regimes such that their sum gives N_t. The variation of the monthly mean concentrations in each of these regimes is shown in the stacked histogram in Figure 10 and the values are listed in Table 1. During August, the accumulation mode concentration dominated the size distribution, contributing almost 45% to N_t, while the nucleation mode contributed just about 20% (Table 1). By September, the scenario has changed with the Aitken mode contributing ~60% to the total. The large decrease in the absolute values in September appears to be associated also with the snowfall event in the early part of the month, which would have largely removed accumulation mode aerosols. This is examined in subsequent sections. During the months of October and November, the distribution appears to remain more or less steady; the nucleation and Aitken modes combined, accounting for ~70 and 60% of the total, probably owing to significant amount of new particle formation in the nucleation regimes, which eventually transforms to higher sizes. Of course in this case, the mass conservation requires that nearly 8 particles in a given size regime have to coagulate to yield one particle with double the size (considering spherical particles) and as such, the share of accumulation mode does not show remarkable changes.

[16] The ratio (N_{ait}/N_{acc}) of Aitken mode concentration to accumulation mode concentration has been used an indicator of the origin and atmospheric processing of the aerosol system [*Komppula et al.*, 2009]. In the absence of new particle formation from precursors this ratio would decrease rapidly as we move farther from major source regions. Over Hanle, our studies have shown that except for the month of August, the ratio N_{ait}/N_{acc} has been much greater than 1, indicating the dominance of Aitken mode over accumulation mode for most of the time (Table 1). Other than new particle formation, precipitation and snowfall would result in an increase the value of N_{ait}/N_{acc}, because wet removal process is more efficient in the accumulation and larger sizes. However, except for a spell of snowfall in the first half of September, the entire period of our study has been devoid of precipitation or snowfall. As such, it appears that new particle formation plays a dominant role in controlling the aerosol size distribution and concentration over Himalayan region. Substantially high values of N_{ait}/N_{acc} (in the range 1–5) have been reported for the free tropospheric atmospheric conditions over high-altitude sites over other regions too [*Weingartner et al.*, 1999; *Nishita et al.*, 2007; *Shaw*, 2007].

5.2. Mean Number-Size Distributions

[17] Using the individual size spectra measured using the SMPS, the monthly mean number-size distributions have been deduced and are shown in Figure 11. The number-size distributions are multimodal in nature, with an "open mode" toward the nucleation size range, and a conspicuous accumulation mode. There is also an indication of a possible coarse mode (size >1000 nm), though it is very weak. Here it should be noted that the distributions are representative of the daytime conditions only, as the instrument could not be operated during nights owing to extreme low temperature, which rendered the condensation nuclei counter nonfunctional. The size distributions shown in Figure 11 are similar to those shown in the work of *Shaw* [2007] for the daytime, who has also reported large changes in the size distributions during nighttime [*Shaw*, 2007, Figure 3], might be associated with the prevalence of clean free-tropospheric conditions and mountain breeze. New particle formation could occur even during nighttime over clean environments as has been reported by *Rissler et al.* [2006], *Russell et al.* [2007], and *Lee et al.* [2008] from different geographical locations. Low volatile organic vapors, if present in the atmosphere, could lead to new particle formation via chemical reactions

Table 1. Monthly Mean Total Concentration and Percentage Share of Each Mode Concentration to the Total

Month (2009)	Total Concentration (N_t) (cm^{-3})	Share of Nucleation Mode to N_t (%)	Share of Aitken Mode to N_t (%)	Share of Accumulation Mode to Total (%)
August	1391.7	22	30	48
September	899.3	11	56	33
October	1180.3	28	42	30
November	1172.0	21	41	38

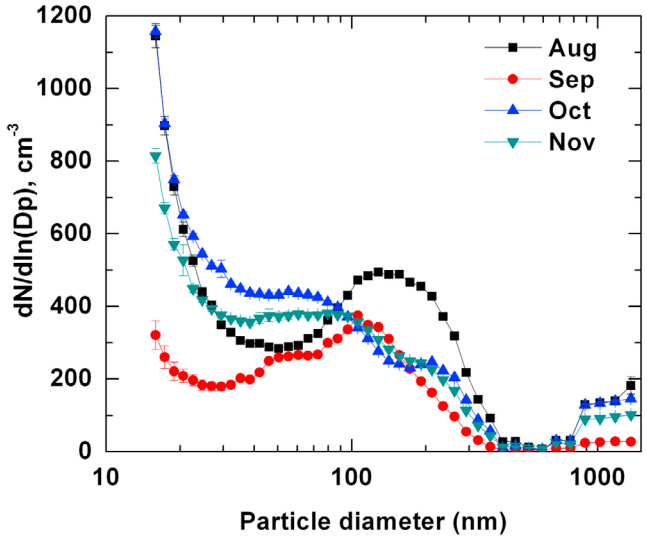

Figure 11. Monthly mean aerosol number-size distributions. Vertical bars through the solid dots indicate the standards.

involving ozone or NO_3 during night in the absence of UV and OH. However, these aspects could not be examined at Hanle owing to lack of observations.

[18] An examination of the time series of the size distribution (Figure 12) revealed that the nucleation mode existed conspicuously until the first week of November (observation number 3000), and weakened thereafter, as the winter conditions advanced. Figure 12 also shows the "growth bananas" from the nucleation events to the accumulation regime in a span of a few days (e.g., from scan 2750 to 3000 in Figure 12). Examining the diurnal variations, *Kulmala et al.* [2004] have reported of "banana-shaped" particle growth in the time evolution of size distribution from the nucleation mode size range to Aitken mode size range, some

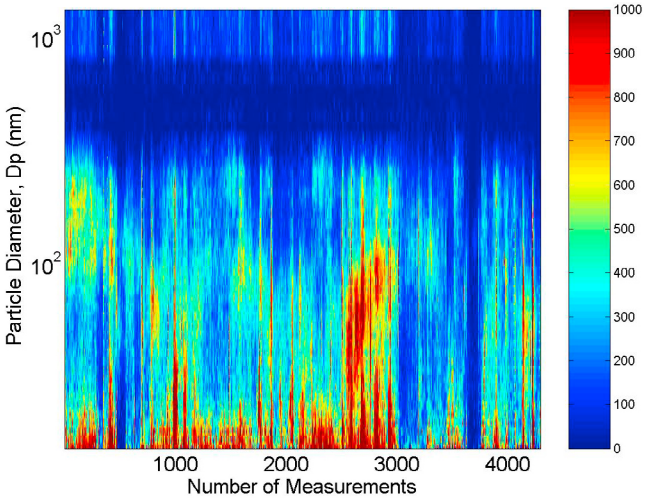

Figure 12. Temporal variation of the size distribution against the number of measurements and particle diameter. A strong nucleation mode can be seen up to the observation number 3000 (which is up to the first week of November).

Table 2. Monthly Mean Accumulation Mode Diameters and Standard Deviations Obtained by Fitting the Lognormal Distribution to the Observed Size Distribution

Month (2009)	Accumulation Mode Diameter (D_{AM})	Geometric Standard Deviation (σ_{AM})	Nucleation Mode Diameter (D_{NU})	Geometric Standard Deviation (σ_{NU})
August	153	1.68		
September	129	1.65	16.5	0.48
October	113	2.18		
November	142	2.27		

time to accumulation mode, which lasts for few hours. In the absence of fresh nucleation events, it is quite possible that such growth continues into accumulation mode in a matter of few days, as seen at Hanle.

[19] By fitting the lognormal distribution (equation (1)) to the monthly mean size distributions, the mode radii and standard deviations were estimated and these are listed in Table 2. The accumulation mode was large and most sharp in August (with mode diameter ~150 nm and standard deviation (σ) 1.68), while it was smallest and broad in October (diameter 113 nm, (σ) 2.18). The nucleation mode was conspicuous (at ~16.5 nm) in September. The values for the accumulation mode diameters obtained in the current study compared well with those of reported by *Shaw* [2007] and *Weingartner et al.* [1999] from mountain top observatories at Mt. Lemmon (2790 m asl). Arizona and a high-alpine site of Jungfraujoch (3580 m asl), respectively. In Table 3 we have compared the summary findings at Hanle with those reported from other high-altitude stations elsewhere, widely separated from the Himalayas. It is interesting to note that, despite the wide differences in the geographic locations of these stations, and the periods of measurements, the modes (diameters and standard deviations) are quite comparable, especially in the accumulation regime, showing the global nature of the particles in the "free troposphere." The difference in the concentrations (such as the least value at Jungfraujoch, despite it being lower than Hanle) might be signifying small spatial heterogeneity that might prevail even at these levels, (for example Jungfraujoch is at higher latitude) and also the difference in the periods of measurements.

[20] With a view to investigating at what diameter the "open mode" becomes well developed and to find out the mode diameter in the nucleation regime, we have operated the CPC in conjunction with UDMA, which covers a size range from 8.9 to 552 nm. The instrument was operated in this configuration for several days during September. The data have been analyzed and the mean picture of the size distribution for possible nucleation events are shown in Figure 13. It is noticed that about 90% of the events occurred in the forenoon hours with the number-size distributions (in 8.9 to 552 nm size range) being bimodal, with a nucleation mode (mode diameter ~16.5) and an accumulation mode (mode diameter 120 nm). The accumulation mode diameter value obtained with UDMA matches well with that of observed with LDMA (Figure 11). However, the nucleation mode was too low to be captured by the LDMA. It is interesting to note that from long-term measurements from high-altitude locations puy de Dome (1465 m

Table 3. A Comparison of the Mean Size Distributions at Hanle With Those Reported for Other High-Altitude Stations Over the Globe

Location	Period	Total Concentration (cm^{-3})	Mode Diameter[a] (nm)	Standard Deviation[a]	Reference
Hanle (32.5°N, 78.5°E, 4520 m)	Aug–Nov	1150	16.5 not resolved 134.3 ± 8.6	1.6 - 1.9 ± 0.2	present study
Jungfraujoch (46.55°N, 7.98°E, 3580 m)	Feb–May	498	38 - 129	2.17 - 1.79	*Weingartner et al.* [1999]
Mt. Lemmon (32.43°N, 100.8°W, 2790 m)	Feb–May	1428	37 - 130	2.03 - 2.2	*Shaw* [2007]
Puy De Dome (45.77°N, 2.95°E, 1465 m)	autumn	1400	17 49 130	1.6 1.7 1.5	*Venzac et al.* [2009]

[a]First, second, and third values given are for the nucleation mode, Aitken mode, and accumulation mode, respectively.

asl) research station, France and Mt. Waliguan, (3816 m asl) in inland China *Venzac et al.* [2009] and *Kivekas et al.* [2009] have shown that the nucleation mode diameter range from 15 to 25 nm, respectively.

5.3. Effect of Snowfall

[21] It was discussed in the earlier sections that, owing to the snowfall episode in the first half of September, the mean N_t values came down in comparison with that of other months. Because snowflakes offer a larger area to capture the airborne particles and scavenge them along the snowfall, snow scavenging is known to be a more efficient removal mechanism than impaction scavenging by precipitation [*Lei and Wania*, 2004; *Sauter and Wang*, 1989; *Chaubey et al.*, 2010]. During September, it can be inferred (from Figure 9) that the contributions of nucleation and accumulation modes to the total concentrations (N_t) remained very low, and seem to be most affected by the snow fall episode, which lasted for several days from 2 to 12 September. The foggy conditions with very high RH (~100%) have inhibited the new particle formation by almost blocking the sunlight and thereby inhibiting the photochemistry during the first half of September thereby reducing the abundance leading to the growth of the accumulation mode. The high RH along with snow fall and precipitation would also lead to wet removal of the close to micron sized accumulation mode particles also. Owing to the above reasons, even though the intense snowfall lasted for about a week, its consequence is clearly reflected even in the monthly mean values (note that there are several hot spots in the N_t values during the second half). A quantitative measurement of the temporal distribution of the snowfall would have been helpful to quantify the amount of particles that might have gone into snow. However, as the snow fall was not anticipated in that season at Hanle, no such measurements could be planned.

5.4. Long-Range Transport

[22] To examine the effect of long-range transport in advecting precursors from inhabited region, 5 day back trajectories arriving at the surface level (500 m above ground level) at Mt. Saraswati, were computed using Hybrid Single Particle Lagrangian Integrated Trajectory (HYSPLIT) Model (see R. R. Draxler and G. D. Rolph, HYSPLIT model access, 2003, available at http://www.arl.noaa/gov/ready/hysplit.html) for all the days of the study period. By performing a cluster analysis [following *Gogoi et al.*, 2009] for each month separately, we have identified the potential pathways and these are shown in Figure 14. The predominant pathways remained from west and far west. On some days the air mass just became southwesterly before arriving at the station (as seen from Figure 3), while on a few occasions the air mass has been of local origin or originated from central Indian regions (Figure 14b). During August, on 70% of the days the air mass at Hanle had arrived from west Asia which could bring in accumulation mode aerosols as well as gaseous precursors. However, N_t tended to be around the highest (~1550 cm^{-3}), whenever the advection was from the central Indian landmass, indicating the effect of anthropogenic aerosols probably directly transported. In September 90% of the times, the air mass was from west Asia, while 10% is from the Indian subcontinent. Unfortunately, owing to the snowfall episode, adequate data are not available during September to arrive at a meaningful statistics. During October all the trajectories were from west Asia, except that the spatial distance covered by the clusters varied. In this month, the N_t values were found to increase with the length of the trajectories, suggesting advection from

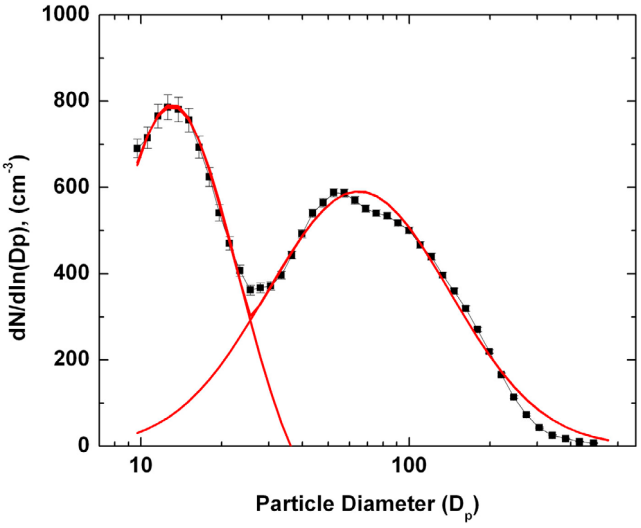

Figure 13. Analytical fits (solid red lines) of the mean number-size distributions.

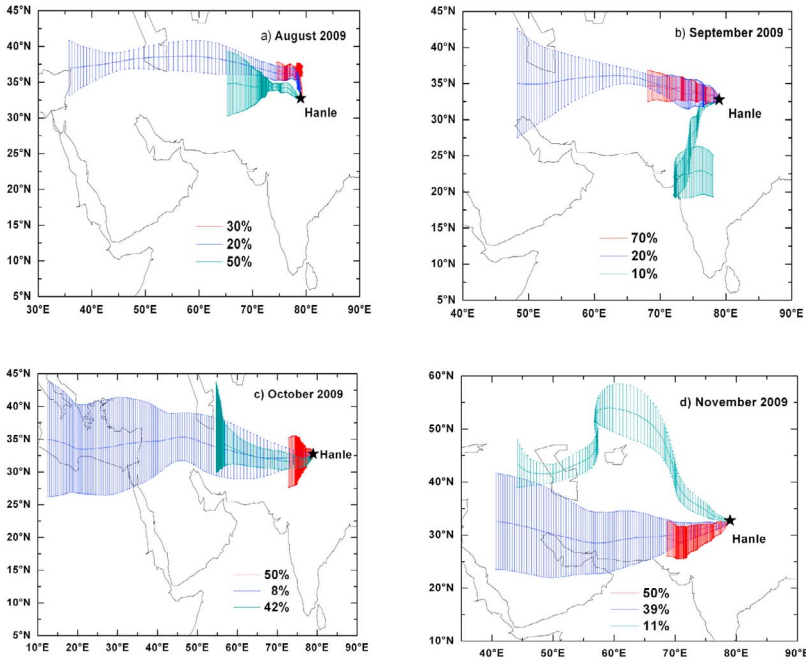

Figure 14. Cluster analysis of the 5 day isentropic back trajectories showing the potential pathways of long-range transport. The predominant transport pathways are from the west and far west of Hanle.

far west being a dominant contributor. It is possible that the precursors are advected along this path and lead to new particle formation over the cool, and moderately humid mountain environment. During November too, 89% of the trajectories were from the west Asian regions, while 11% were from the northwest of the measurements site. The accumulation mode basically arises from cloud cycling involving multiple condensation and evaporation processes. Though the cluster analyses indicated that most of the time, the air mass trajectories arriving at Hanle during the study period had long overpass over dry west Asian desert regions, the presence of abundance of clouds over the Western and Trans-Himalayan regions during this season (associated with the Asian monsoon in the southern plains) would be conducive for cloud processing. The presence of lots of frequently occurring cloud patches was noticed by the authors during the observation periods. These clouds drifted rapidly across the mountains, nevertheless sparsely precipitated, again suggesting cloud processing. The strong convection in the southern plains, though would be efficient in lifting the polluted air from the Indo-Gangetic Plains (IGP), they seldom reach Hanle, primarily owing to the westerly nature of the prevailing winds and being orographically blocked by the tall south Himalayan ranges. This is also evidenced by the trajectory clusters in Figure 14. Here, it should be noted that, as the winter conditions strengthen (average temperature going below 0°C), convective activities would be become weak and nonconducive for long-range transport. Nevertheless, N_t values remained higher associated with west Asian air mass, and lower (~950 cm^{-3}) whenever the trajectories were from the northwest.

5.5. Summary

[23] As a part of ISRO-RAWEX field campaign, an aerosol observatory has been set up at a high-altitude Himalayan site (Hanle) and extensive campaign mode measurements of aerosol number-size distributions have been carried using an SMPS, covering nucleation, Aitken and accumulation regimes. The major findings are:

[24] 1. The total particle number concentration varied over a wide range, from as low as 80 to 8000 cm^{-3} with a mean value of ~1150 ± 500 cm^{-3}. It was well comparable to those reported from other Himalayan sites.

[25] 2. The mean number-size distributions depicted bimodal structure, with an accumulation mode in the range 115 to 150 nm and a nucleation mode at ~17 nm.

[26] 3. Strong signatures of new particle formation (apparently driven by photochemistry) were seen during the forenoon hours of September, October and November, with the time of occurrence of the peak shifting gradually to later parts of the forenoon as the days advanced more and more toward winter, and the solar elevation decreased.

[27] 4. The trajectory cluster analysis showed that the predominant air mass pathway is from the west Asia, which might be bringing in accumulation mode particles of Arabian origin and precursor gases over the site, which might be favoring the new particle formation through photochemistry.

[28] 5. Large decrease in (1) the total number concentration, (2) geometric mean diameter and (3) contribution from the nucleation and accumulation mode to the total concentration was noticed associated with a strong and extended snowfall episode during the first half of September. It appears that the removal of accumulation mode particles by snow scavenging and inhibition of new particle formation by the adverse meteorological conditions contributed to this.

[29] **Acknowledgments.** This work is a part of the RAWEX field campaign under the ISRO-GBP-ARFI project. We acknowledge the director of IIA for providing the facilities necessary to carry out the campaign.

The authors wish to thank the technical and civil staff of the IIA observatory, Hanle, headed by Dorje Angchuk, for their logistic support throughout the campaign.

References

Babu, S. S., S. K. Satheesh, K. K. Moorthy, C. B. S. Dutt, V. S. Nair, D. P. Alappattu, and P. K. Kunhikrishnan (2008), Aircraft measurements of aerosol black carbon from a coastal location in the north-east part of peninsular India during ICARB, *J. Earth Syst. Sci.*, *117*, 263–271, doi:10.1007/s12040-008-0030-1.

Babu, S. S., K. K. Moorthy, and S. K. Satheesh (2010), Vertical and horizontal gradients in aerosol black carbon and its mass fraction to composite aerosols over the east coast of peninsular India from Aircraft measurements, *Adv. Meteorol.*, *2010*, 812075, doi:10.1155/2010/812075.

Brown, S. S., et al. (2006), Nocturnal odd-oxygen budget and its implications for ozone loss in the lower troposphere, *Geophys. Res. Lett.*, *33*, L08801, doi:10.1029/2006GL025900.

Chaubey, J. P., K. K. Moorthy, S. S. Babu, V. S. Nair, and A. Tiwari (2010), Black carbon aerosols over coastal Antarctica and its scavenging by snow during the Southern Hemispheric summer, *J. Geophys. Res.*, *115*, D10210, doi:10.1029/2009JD013381.

Collins, D. R., D. R. Cocker, R. C. Flagan, and J. H. Seinfeld (2004), The scanning DMA transfer function, *Aerosol Sci. Technol.*, *38*, 833–850, doi:10.1080/027868290503082.

Fan, J., R. Zhang, G. Li, W.-K. Tao, and X. Li (2007), Simulations of cumulus clouds using a spectral microphysics cloud-resolving model, *J. Geophys. Res.*, *112*, D04201, doi:10.1029/2006JD007688.

Gajananda, K., J. C. Kuniyal, G. A. Momin, P. S. P. Rao, P. D. Safai, S. Tiwan, and K. Ali (2005), Trend of atmospheric aerosols over the north western Himalayan region, India, *Atmos. Environ.*, *39*, 4817–4825, doi:10.1016/j.atmosenv.2005.01.038.

Gogoi, M. M., K. K. Moorthy, S. S. Babu, and P. K. Bhuyan (2009), Climatology of columnar aerosol properties and the influence of synoptic conditions: First-time results from the northeastern region of India, *J. Geophys. Res.*, *114*, D08202, doi:10.1029/2008JD010765.

Hamed, A., et al. (2011), The role of relative humidity in continental new particle formation, *J. Geophys. Res.*, *116*, D03202, doi:10.1029/2010JD014186.

Jiang, H., and G. Feingold (2006), Effect of aerosol on warm convective clouds: Aerosol-cloud-surface flux feedbacks in a new coupled large eddy model, *J. Geophys. Res.*, *111*, D01202, doi:10.1029/2005JD006138.

Kivekas, N., et al. (2009), Long term particle size distribution measurements at Mount Waliguan, a high altitude site in inland China, *Atmos. Chem. Phys.*, *9*, 5461–5474, doi:10.5194/acp-9-5461-2009.

Komppula, M., H. Lihavainen, A.-P. Hyvärinen, V.-M. Kerminen, T. S. Panwar, V. P. Sharma, and Y. Viisanen (2009), Physical properties of aerosol particles at a Himalayan background site in India, *J. Geophys. Res.*, *114*, D12202, doi:10.1029/2008JD011007.

Kulmala, M., H. Vehkamaki, T. Petaja, M. Dal Maso, A. Lauri, V.-M. Kerminen, W. Birmili, and P. H. McMurry (2004), Formation and growth rates of ultrafine atmospheric particles: A review of observations, *J. Aerosol Sci.*, *35*, 143–176, doi:10.1016/j.jaerosci.2003.10.003.

Lau, K.-M., and K.-M. Kim (2006), Observational relationships between aerosol and Asian monsoon rainfall, and circulation, *Geophys. Res. Lett.*, *33*, L21810, doi:10.1029/2006GL027546.

Lau, K.-M., M. K. Kim, and K. M. Kim (2006), Aerosol induced anomalies in the Asian summer monsoon—The role of the Tibetan Plateau, *Clim. Dyn.*, *26*, 855–864, doi:10.1007/s00382-006-0114-z.

Lee, T., X. Y. Yu, S. M. Kreidenweis, W. C. Malm, and J. L. Collet (2008), Semi-continuous measurement of PM2.5 ionic composition at several rural locations in the United States, *Atmos. Environ.*, *42*, 6655–6669, doi:10.1016/j.atmosenv.2008.04.023.

Lei, Y. D., and F. Wania (2004), Is rain or snow a more efficient scavenger of organic chemicals?, *Atmos. Environ.*, *38*, 3557–3571, doi:10.1016/j.atmosenv.2004.03.039.

Moorthy, K. K., S. K. Satheesh, S. S. Babu, and C. B. S. Dutt (2008), Integrated campaign for aerosols, gases and radiation budget (ICARB): An overview, *J. Earth Syst. Sci.*, *117*, 243–262, doi:10.1007/s12040-008-0029-7.

Murugavel, P., V. Gopalakrishnan, V. Pant, and A. K. Kamra (2008), Airborne measurements of submicron aerosols across the coastline at Bhubaneswar during ICARB, *J. Earth Syst. Sci.*, *117*, 273–280, doi:10.1007/s12040-008-0020-3.

Nishita, C., K. Osada, K. Matsunaga, and Y. Iwasaka (2007), Number-size distributions of free tropospheric aerosol particles at Mt. Norikura, Japan: Effects of precipitation and air mass transportation pathways, *J. Geophys. Res.*, *112*, D10213, doi:10.1029/2006JD007969.

Raes, F., R. Van Dingenen, E. Cuevas, P. F. J. Van Velthoven, and J. M. Prospero (1997), Observations of aerosols in the free troposphere and marine boundary layer of the subtropical Northeast Atlantic: Discussion of processes determining their size distribution, *J. Geophys. Res.*, *102*, 21,315–21,328.

Raes, F., R. Van Dingenen, E. Vignati, J. Wilson, J.-P. Putaud, J. H. Seinfeld, and P. Adams (2000), Formation and cycling of aerosols in the global troposphere, *Atmos. Environ.*, *34*, 4215–4240, doi:10.1016/S1352-2310(00)00239-9.

Reischl, G. P. (1991), Measurement of ambient aerosols by the differential mobility analyzer method: Concepts and realization criteria for the size range between 2 and 500 nm, *Aerosol Sci. Technol.*, *14*, 5–24, doi:10.1080/02786829108959467.

Remer, L. A., et al. (2009), Executive summary, in *Atmospheric Aerosol Properties and Climate Impacts: A Report by the U.S. Climate Change Science Program and the Subcommittee on Global Change Research*, edited by M. Chin, R. A. Kahn, and S. E. Schwartz, pp. 1–8, Natl. Aeronaut. and Space Admin., Washington, D. C.

Rissler, J., A. Vestin, E. Swietlicki, G. Fisch, J. Zhou, P. Artaxo, and M. O. Andreae (2006), Size distribution and hygroscopic properties of aerosol particles from dry-season biomass burning in Amazonia, *Atmos. Chem. Phys.*, *6*, 471–491, doi:10.5194/acp-6-471-2006.

Russell, P. B., et al. (2007), Multi-grid-cell validation of satellite aerosol property retrievals in INTEX/ITCT/ICARTT 2004, *J. Geophys. Res.*, *112*, D12S09, doi:10.1029/2006JD007606.

Satheesh, S. K., K. K. Moorthy, S. Suresh Babu, V. Vinoj, and C. B. S. Dutt (2008), Climate implications of large warming by elevated aerosol over India, *Geophys. Res. Lett.*, *35*, L19809, doi:10.1029/2008GL034944.

Satheesh, S. K., V. Vinoj, S. S. Babu, K. K. Moorthy, and V. S. Nair (2009a), Vertical distribution of aerosols over the east coast of India inferred from airborne LIDAR measurements, *Ann. Geophys.*, *27*, 4157–4169, doi:10.5194/angeo-27-4157-2009.

Satheesh, S. K., K. Krishna Moorthy, S. Suresh Babu, V. Vinoj, V. S. Nair, S. Naseema Beegum, C. B. S. Dutt, D. P. Alappattu, and P. K. Kunhikrishnan (2009b), Vertical structure and horizontal gradients of aerosol extinction coefficients over coastal India inferred from airborne lidar measurements during the Integrated Campaign for Aerosol, Gases and Radiation Budget (ICARB) field campaign, *J. Geophys. Res.*, *114*, D05204, doi:10.1029/2008JD011033.

Sauter, D. P., and K. P. Wang (1989), An experimental study of the scavenging of aerosol particles by natural snow crystals, *J. Atmos. Sci.*, *46*, 1650–1655, doi:10.1175/1520-0469(1989)046<1650:AESOTS>2.0.CO;2.

Sellegri, K., P. Laj, H. Venzac, J. Boulon, D. Picard, P. Villani, P. Bonasoni, A. Marinoni, P. Cristofanelli, and E. Vuillermoz (2010), Seasonal variations of aerosol size distributions based on long-term measurements at the high altitude Himalayan site of Nepal Climate Observatory-Pyramid (5079 m), Nepal, *Atmos. Chem. Phys. Discuss.*, *10*, 6537–6566.

Shaw, G. E. (2007), Aerosols at a mountaintop observatory in Arizona, *J. Geophys. Res.*, *112*, D07206, doi:10.1029/2005JD006893.

Vaattovaara, P., et al. (2009), The evolution of nucleation- and Aitken mode particle compositions in a boreal forest environment during clean and pollution-affected new-particle formation events, *Boreal Environ. Res.*, *14*, 662–682.

Venzac, H., K. Sellegri, P. Villani, D. Picard, and P. Laj (2009), Seasonal variation of aerosol size distributions in the free troposphere and residual layer at the puy de Dome station, France, *Atmos. Chem. Phys.*, *9*, 1465–1478, doi:10.5194/acp-9-1465-2009.

Verma, N., S. P. Bagare, S. S. Nigombam, and R. B. Singh (2009), Aerosol optical properties retrieved using sky radiometer at Hanle in western Himalayas, *J. Atmos. Sol. Terr. Phys.*, *72*, 115–124, doi:10.1016/j.jastp.2009.10.016.

Weber, R. J., P. H. McMurry, F. L. Eisele, and D. J. Tanner (1995), Measurement of expected nucleation precursor species and 3–500 nm diameter particles at Mauna Loa Observatory, Hawaii, *J. Atmos. Sci.*, *52*, 2242–2257, doi:10.1175/1520-0469(1995)052<2242:MOENPS>2.0.CO;2.

Weingartner, E., S. Nyeki, and U. Baltensperger (1999), Seasonal and diurnal variation of aerosol size distributions ($10 < D < 750$ nm) at a high-Alpine site (Jungfraujoch 3580 m asl), *J. Geophys. Res.*, *104*, 26,809–26,820, doi:10.1029/1999JD900170.

S. P. Bagare, B. C. Bhatt, V. K. Gaur, T. P. Prabhu, and N. S. Singh, Indian Institute of Astrophysics, Sarjapur Road, Bangalore 560034, India.

M. M. Gogoi, S. Kumar Kompalli, K. K. Moorthy, J. Prakash Chaubey, V. Sreekanth, and S. Suresh Babu, Space Physics Laboratory, Vikram Sarabhai Space Centre, Trivandrum 695022, India. (krishnamoorthyspl@gmail.com)